JACS
JOURNAL OF THE AMERICAN CHEMICAL SOCIETY
pubs.acs.org/JACS
Article

Synthesis and Characterization of U≡C Triple Bonds in Fullerene Compounds

Yang-Rong Yao, Jing Zhao, Qingyu Meng, Han-Shi Hu, Min Guo, Yingjing Yan, Jiaxin Zhuang, Shangfeng Yang, Skye Fortier, Luis Echegoyen, W. H. Eugen Schwarz, Jun Li,* and Ning Chen*

Cite This: J. Am. Chem. Soc. 2023, 145, 25440−25449

Read Online

ACCESS | Metrics & More | Article Recommendations | Supporting Information

ABSTRACT: Despite decades of efforts, the actinide−carbon triple bond has remained an elusive target, defying synthesis in any isolable compound. Herein, we report the successful synthesis of uranium−carbon triple bonds in carbide-bridged bimetallic [U≡C−Ce] units encapsulated inside the fullerene cages of C_{72} and C_{78}. The molecular structures of UCCe@C_{2n} and the nature of the U≡C triple bond were characterized through X-ray crystallography and various spectroscopic analyses, revealing very short uranium−carbon bonds of 1.921(6) and 1.930(6) Å, with the metals existing in their highest oxidation states of +6 and +4 for uranium and cerium, respectively. Quantum-chemical studies further demonstrate that the C_{2n} cages are crucial for stabilizing the [U^{VI}≡C−Ce^{IV}] units through covalent and coordinative interactions. This work offers a new fundamental understanding of the elusive uranium−carbon triple bond and informs the design of complexes with similar bonding motifs, opening up new possibilities for creating distinctive molecular compounds and materials.

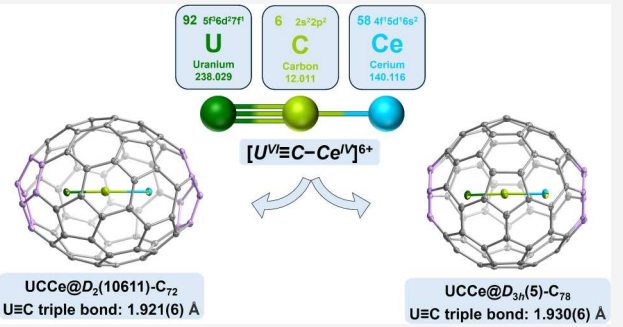

INTRODUCTION

The actinides are technologically important elements, where the understanding of their fundamental chemical properties and roles in the nuclear fuel cycle is critical for advancing nuclear technology,[1] which is important for building a diverse portfolio of carbon-free energy sources. Yet, despite this, the chemistry of the actinide series remains underdeveloped in comparison to transition metals and main group elements. Major in-roads into the understanding of the electronic properties and chemistry of the transition metals have been accomplished over the decades through the synthesis of molecular compounds possessing metal−ligand multiple bonds,[2] where the critical understanding of d-orbital participation in bonding motifs and reactivity has been elucidated. While extensive studies of the uranyl cation, [O≡U≡O]$^{2+}$, have shown the 5f orbitals to play a critical role in the formation of the formal uranium−oxygen triple bonds,[3−5] 5f orbital participation in other U═E and U≡E bonding remains less clear and an intensive area of study.[6−9] Indeed, efforts into the synthesis of uranium and actinide metal−ligand multiple bonds have intensified over the past two decades, with significant advances achieved in the synthesis of a variety of carbeno,[10−13] imido,[14−17] nitrido,[18,19] heavier-pnictogenido,[20−22] oxo,[23−26] and chalcogenido complexes.[27−29]

Notable is the progress that has been made in developing methods for the synthesis of new actinide−ligand multiple bonds. Yet, a significant gap exists in the domain of molecular actinide complexes possessing the so-called "true" alkylidene and alkylidyne bonds that are not stabilized through the possible heteroatom resonance contributions.[30] Pioneering matrix isolation experiments identified transient uranium methylidyne molecules X_3U≡CH (X = F, Cl, Br)[31] and uranium carbides such as U≡C and C≡U≡C.[32] However, these molecules have been observed only through spectroscopic methods at low temperatures in noble-gas matrices and studied theoretically. A recent report shows that the use of a novel alkylidene transfer reagent leads to the isolation of the actinide allenylidenes possessing small but significant An═C═C═CPh_2 (An = Th, U) resonance contributions,[33] which is highly promising as it shows that actinide−carbon multiple bonds may potentially be synthetically accessible under less specialized laboratory conditions. The difficulty in isolating actinide−carbon multiple bonds is thought to arise from high bond polarization and orbital energy mismatch that lead to poor An−C π-overlap.[34]

Received: September 12, 2023
Revised: October 31, 2023
Accepted: November 1, 2023
Published: November 13, 2023

https://doi.org/10.1021/jacs.3c10042
J. Am. Chem. Soc. 2023, 145, 25440−25449

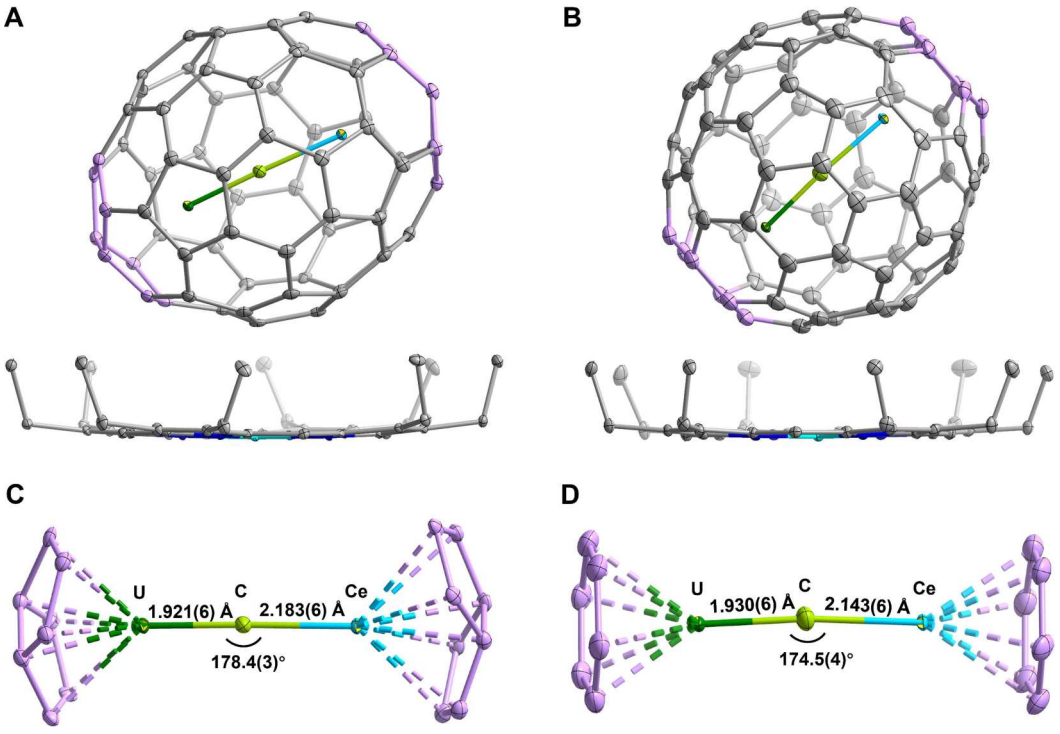

Figure 1. Oak Ridge thermal ellipsoid plots (ORTEP) of the predominant crystal conformations, drawn at 20% ellipsoids. *Left*: (A and C): UCCe@D_2(10611)-C_{72}. *Right*: (B and D): UCCe@D_{3h}(5)-C_{78}. *Top* (A and B): triatomic unit inside the fullerene cage above the cocrystallized Ni^{II}(OEP) molecule; all solvent molecules and hydrogen atoms are omitted. *Bottom* (C and D): endohedral unit with the sandwiching parts of the cage, interatomic distances in Å, and central bond angle in °.

In an effort to counter the high reactivity of actinide fragments possessing unusual bonding motifs, we have successfully employed the capture and stabilization of such moieties within fullerene cages.[35−42] The hollow cavity encloses the fragments, preventing further reactivity, while the cage carbon atoms provide additional coordinative support to the metal center. In 2018, we reported the unprecedented isolation of the uranium endohedral metallofullerene U_2C@C_{80} that contains a remarkable U═C═U unit.[35] Characterization of its molecular structure through X-ray crystallography revealed short U═C bonds (2.03 Å) with an unusual U═C═U bending angle of 142.8(3)°, where a poor π-overlap leads to a significant charge accumulation on the carbide atom with a partial donation of the density into a U 5f/6d-hybrid orbital. Utilizing the fullerene capture, we recently reported the synthesis and characterization of USc_2C_2@C_{80} and USc_2NC@C_{80}, where electronic analysis indicates C═U═C and C═U═N bonding motifs possessing triple-bond resonance contributions.[41]

In this work, we report the synthesis and characterization of endohedral metallofullerenes (EMFs) UCCe@C_{2n} ($2n$ = 72 and 78) containing the first structurally characterized uranium−carbon triple bonds (U≡C) in a stable and isolable form. The mixed, bimetallic [U≡C−Ce] carbide cluster contains uranium and cerium in their highest oxidation states of +6 and +4, respectively. Through X-ray crystallographic analyses, the structural characterization unveils the shortest uranium−carbon bonds ever recorded to date, measuring 1.921(6) and 1.930(6) Å, encapsulated within the C_{72} and C_{78} cages, respectively. The nature of the U≡C triple bond is investigated by ultraviolet−visible, infrared, and X-ray absorption spectroscopy analyses, as well as by quantum-theoretical analyses.

RESULTS AND DISCUSSION

Synthesis and Molecular Structures of UCCe@C_{2n}. UCCe@C_{72} and UCCe@C_{78} were synthesized by a modified Krätschmer−Huffman direct-current arc-discharge method.[43] A drilled graphite rod, packed with a mixture of U_3O_8, graphite powder, and CeO_2 (in molar ratios of U:C:Ce = 1:24:1), was installed in an arcing reactor as the anode under a 200 Torr He atmosphere, and then arced with a graphite cathode at 100 A direct current, yielding the products in the carbon soot. The two targeted U-based metallofullerenes were extracted from the carbon soot by the CS_2 solvent for 24 h and then isolated by multistep high-performance liquid chromatography (HPLC), as illustrated in Figures S1 and S2. The high purity of the two metallofullerenes was confirmed by chromatograms and mass spectra (Figure S3). Importantly, all the experimental isotopic distributions of the two metallofullerenes agree well with the theoretical simulation, providing strong confirmation of their elemental composition.

The molecular structures of the two EMFs (Figure 1) were unambiguously determined as UCCe@D_2(10611)-C_{72} and UCCe@D_{3h}(5)-C_{78} by cocrystallization with Ni^{II}(OEP) (OEP = 2, 3, 7, 8, 12, 13, 17, 18-octa-ethyl-porphyrin dianion, a crystallization promoter to improve the crystallization of the EMFs and hinder the rotation of the fullerene cages) via solid $\pi-\pi$ interactions. Notably, UCCe@D_2(10611)-C_{72} represents the case of a cluster encapsulated into the chiral D_2(10611)-C_{72}, which does not obey the well-known Isolated Pentagon Rule (IPR) proposed by Kroto.[44] D_2 and D_{3h} represent the symmetry of the isolated fullerene cages, and the numbers in parentheses are their isomeric codes.[45] Both cocrystals crystallized in the monoclinic space group $P2_1/c$ with one EMF&Ni^{II}(OEP) adduct in the asymmetric unit (Table S1).

https://doi.org/10.1021/jacs.3c10042
J. Am. Chem. Soc. 2023, 145, 25440−25449

Table 1. Geometric Parameters of UCCe Inside C_{2n} ($2n$ = 72 and 78) and between Two Ligands (L = H_3 or C_7H_7)[a]

species	bond lengths				bond angles
	L[b]−U	U≡C	C−Ce	Ce−L[b]	U−C−Ce
UCCe@C_{72}	2.49 ± 0.03 (2.51)	**1.921 ± 0.006 (1.91)**	2.183 ± 0.006 (2.20)	2.58 ± 0.03 (2.58)	178.4 ± 0.3 (179.5)
UCCe@C_{78}	2.43 ± 0.03 (2.48)	**1.930 ± 0.006 (1.90)**	2.143 ± 0.006 (2.17)	2.46 ± 0.03 (2.55)	174.5 ± 0.3 (174.7)
H_3>UCCe<H_3	(1.99)	**(1.88)**	(2.31)	(2.03)	(178.4)
C_7H_7>UCCe<C_7H_7	(2.55)	**(1.89)**	(2.38)	(2.55)	(180.0)

[a]For the distances of U or Ce from the various adjacent ligand atoms, the mean values are given with standard deviations. Bond lengths (in Å) and bond angles (in °) are from X-ray diffraction of UCCe@C_{2n}·[Ni-OEP] cocrystals and from the PBE/TZ2P calculation (in parentheses) of UCCe@C_{2n} and L>UCCe<L (> and < indicate the multiple dative bond pairs). [b]L for UCCe@C_{72} is the pentalene portion, for UCCe@C_{78} is the benzene portion, for H_3>UCCe<H_3 is H_3, for C_7H_7>UCCe<C_7H_7 is the carbon ring. The present fullerene ligands, $D_2(10611)$-C_{72} and $D_{3h}(5)$-C_{78}, can formally accept six electrons, forming a closed-shell electronic structure. In order to substitute the fullerene cage with smaller ligands (L) with similar electronegativity and similar electron-accepting abilities for the calculations, we chose two pairs of small ligands (L = H_3 and C_7H_7), each of which can accept three electrons and then form a sandwich-like configuration with a closed-shell $(L)^{3-}$>$(UCCe)^{6+}$<$(L)^{3-}$ electronic structure. The U≡C triple bond length hardly changes when the rigid fullerene cage is replaced by the two freely moving and sandwiching clusters of H_3 or C_7H_7.

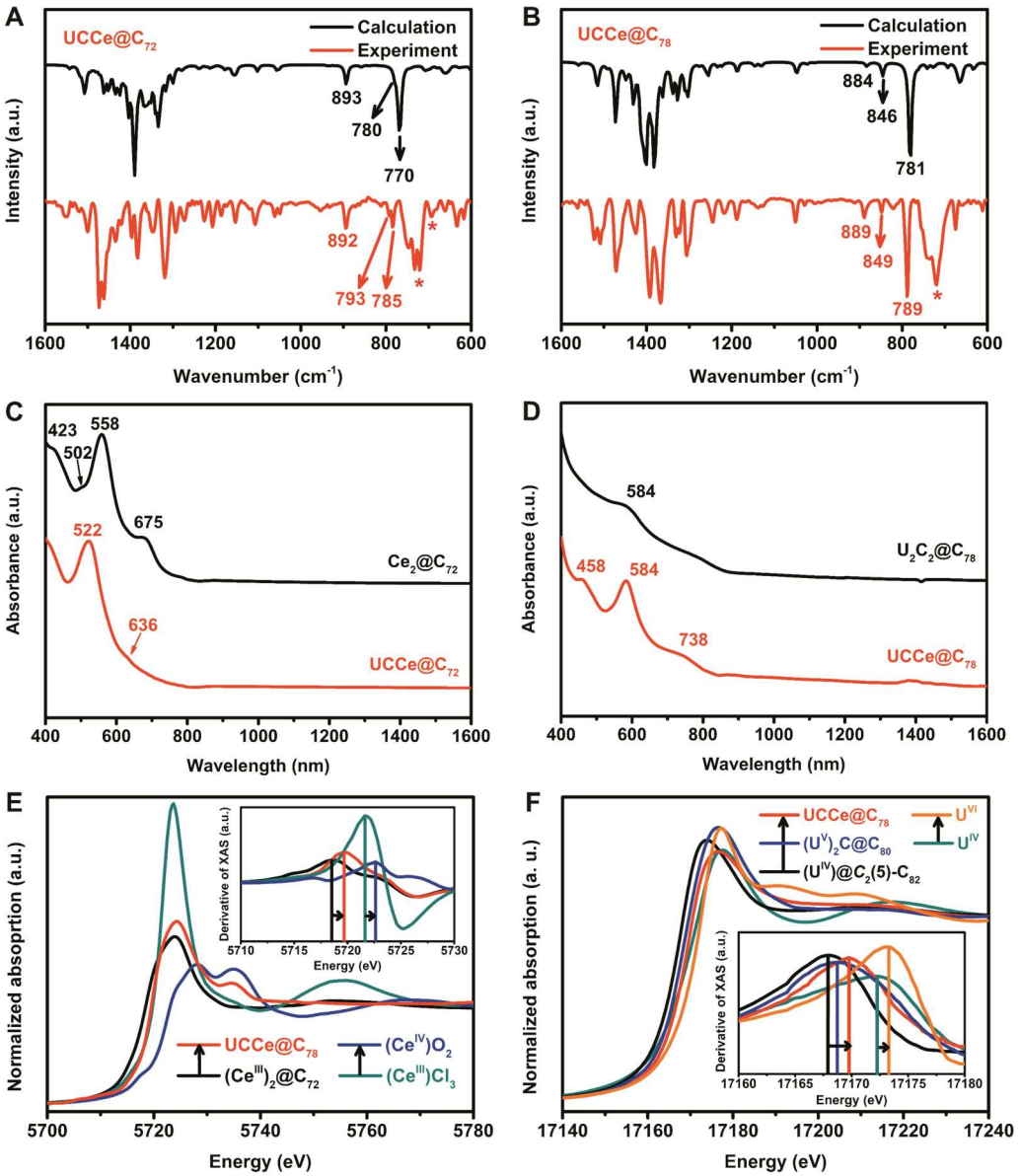

Figure 2. IR, vis−NIR, and XAS results of UCCe@C_{2n}. *Top:* experimental (solid state, ambiance) and simulated (gas state, vacuum) FTIR spectra of (A) UCCe@C_{72} and (B) UCCe@C_{78} (the peaks of the residue toluene are marked with asterisks). *Middle*: comparison of vis−NIR absorption spectra (C) of UCCe@$D_2(10611)$-C_{72} with Ce_2@$D_2(10611)$-C_{72} and (D) of UCCe@$D_{3h}(5)$-C_{78} with U_2C_2@$D_{3h}(5)$-C_{78}. *Bottom*: comparison of L_3-edge XAS of UCCe@C_{78} (E) for Ce-2$p_{3/2}$ with $Ce^{IV}O_2$, $Ce^{III}{}_2$@C_{72}, and $Ce^{III}Cl_3$, and (F) for U-2$p_{3/2}$ with uranyl(U^{VI})-dinitrate, $U^{V}{}_2C$@C_{80}, U^{IV}@$C_2(5)$-C_{82}, and uranium(U^{IV}) disulfate; *inserts*: derivative spectra highlighting the 'edge energies' of the first peaks by vertical lines.

https://doi.org/10.1021/jacs.3c10042
J. Am. Chem. Soc. 2023, 145, 25440−25449

The two EMFs comprise two cage orientations with similar occupancies (Table S2 and Figures S4−5), suggesting that the two orientations coexist in the cocrystals (see Supporting Information).

Crystallographic disorder within EMF cages and clusters is commonplace, but in the cases of UCCe@C_{72} and UCCe@C_{78}, the central carbon atom is fully ordered and provides a clear anchoring point. In UCCe@C_{72}, the cluster exhibits a nearly fully ordered arrangement of uranium and cerium atoms, for which the major metal sites refine well to 86% occupancy with very good refinement parameters in the crystallographic model. Conversely, while disorder within the cluster is more apparent in UCCe@C_{78}, it still exhibits a significant component with 58% site occupancy for the uranium and cerium atoms (Table S3).

In UCCe@C_{72}, each of the U and Ce atoms possesses η^8-coordination to pentalene fragments of the cage, forming metal−carbon bond distances of 2.4−2.6 Å, with cerium exhibiting slightly longer Ce−C bonds within this range. On the other hand, each of the metal atoms in UCCe@C_{78} is η^6-coordinated to the C_6-rings of the C_{78} cage. The UCCe clusters are nearly linear with the measured U−C−Ce angles of 178.4(3) and 174.5(3)° situated on the long twofold axis of D_2(10611)-C_{72} and threefold axis of D_{3h}(5)-C_{78}, respectively. Furthermore, all the interatomic distances and angles, including the bond lengths of C_{cage}−U, Ce−C_{cage}, C−Ce, and the U−C−Ce angles in the theoretically optimized spin-singlet UCCe@C_{2n} molecules (*vide infra*), fit well with the experimental values (Tables 1 and S4). For example, the C−Ce distances in C_{72} and C_{78} are measured as 2.183(6) and 2.143(6) Å, in good agreement with the calculated values (2.20 and 2.17 Å) but shorter than the sum of the single-bond covalent radii of Ce and C (2.38 Å).[46]

The most salient feature of the two EMFs is the very short U−C bond lengths, measured as 1.921(6) and 1.930(6) Å inside C_{72} and C_{78}, respectively, which are well below the sum of the covalent U=C double bond radii (2.01 Å).[46] This is far shorter than the U=C distance in the methanide-coordinated U(VI) oxo carbene complex ([O=U=CR_2]Cl_2) (2.184(3) Å),[11] which exhibits a double-bond character enhanced through the inverse trans influence contributions with the oxo atom.[11] As would be expected with a higher U≡C bond order, the U−C bonds in UCCe@C_{72} and UCCe@C_{78} are significantly shorter than the U=C=U bonds in U_2C@C_{80} (2.028(5) and 2.033(5) Å)[35] and also shorter than the U=C bond lengths of 2.060(1) to 2.163(4) Å in USc_2C_2@C_{80} that results from the multiple and pronounced multicentric bonding character of its cluster.[41] Furthermore, the U−C bond distances of the UCCe moieties are comparable to the computed distances of $X_3U{\equiv}CH$ molecules (1.90−1.94 Å; X = H or halogen)[31] and only slightly longer than those computed for the matrix isolated species U≡C and C≡U≡C (1.86 and 1.83 Å).[32] On top of this, the experimentally determined distances agree well with the U−C bond lengths calculated for UCCe@C_{72} and UCCe@C_{78} (Table 1). Altogether, these results provide strong and compelling evidence of the presence of a genuine U≡C bond, the first of its kind in an isolable molecular system.

Spectroscopic Properties of UCCe@C_{2n}. To support the unique structural parameters of UCCe@C_{2n} and investigate the bonding nature of the encapsulated UCCe units, spectroscopic studies, including Fourier transform infrared (FTIR) absorption spectroscopy, visible near-infrared (vis−NIR) absorption spectroscopy, and X-ray absorption near-edge structure (XANES) spectroscopy, were performed. As shown in Figure 2A,B, the experimental FTIR absorption spectra of UCCe@C_{2n} are in good agreement with the corresponding calculated ones. These spectra exhibit two bands of fullerene vibrations, with one ranging from 1600 to 1000 cm^{-1} and the other below 900 cm^{-1}, separated by a gap of approximately 100 cm^{-1} in between, which is consistent with previous studies.[47] In addition, the endohedral triatomic U≡C−Ce unit contributes nine modes, eight of which are very weak due to the heavy metal atoms and are located between approximately 50 and 200 cm^{-1}. These modes include three translational rocking modes, two torsional wagging modes, two bending modes, and one symmetrical stretching mode, all with low IR intensity. The more intense 'asymmetric stretching' of the central C atom between the two heavy metal atoms is near 800 cm^{-1}, coupling with near-degenerate fullerene vibration modes and resulting in split bands. Calculations reveal that for UCCe@C_{72}, there is one stronger (770 cm^{-1}) and one weaker (780 cm^{-1}) feature with an asymmetric C stretching admixture, while for UCCe@C_{78}, there is one stronger feature (781 cm^{-1}) and one weak peak nearby (846 cm^{-1}).

vis−NIR absorption spectra of EMFs are known to be dominated by the $\pi \rightarrow \pi^*$ transitions of the carbon cages and are sensitive to the cage isomerism, degree of charge transfer, and covalent-overlap interactions between the fullerene cage and the endo units.[48] As shown in Figure 2C, UCCe@D_2(10611)-C_{72} presents an overall similar absorption profile as Ce_2@D_2(10611)-C_{72}.[49] The absorption spectrum of UCCe@D_{3h}(5)-C_{78} features a strong peak at 584 nm and two broad shoulders on both sides at 458 and 738 nm, which bears an overall resemblance to that of U_2C_2@D_{3h}(5)-C_{78} (Figure 2D).[36] The Ce_2 and U_2C_2 endo units populate the lowest three adjacent virtual orbitals of D_2(10611)-C_{72}[49] and D_{3h}(5)-C_{78}.[36] Accordingly, it appears reasonable to assume that the electronic configurations of UCCe@C_{72} and UCCe@C_{78} are formally $[UCCe]^{6+}$@$[C_{2n}]^{6-}$, with the metal atoms in their highest formal oxidation states, U^{6+} and Ce^{4+}, brought together by a bridging C atom using four bonding electron pairs (formally C^{4-}).

Notably, a comparison of vis-NIR spectra between UCCe@C_{72} and Ce_2@C_{72}, as well as that between UCCe@C_{78} and U_2C_2@C_{78}, reveals two noteworthy distinctions. First, substituting a U_2C_2 cluster with a UCCe cluster inside the C_{78} cage does not result in any spectral peak shift. However, replacing a Ce_2 dimer with a UCCe cluster within the C_{72} cage leads to a blue shift for the major absorption peaks, with the peaks shifting from 558 to 522 nm and from 675 to approximately 636 nm. This shift suggests that the introduction of the encapsulated U has likely contributed to the molecular orbitals of the carbon cages. Second, the introduction of U into the encapsulated moieties results in broader vis-NIR spectra. For instance, while the absorption spectrum of U_2C_2@C_{78} exhibits an overall resemblance to that of UCCe@C_{78}, the absorption peaks are broader in the former, with the 458 and 738 nm peaks in UCCe@C_{78} becoming flattened in the U_2C_2@C_{78} spectrum. A similar phenomenon is observed in the UCCe@C_{72} spectrum, where the 502 nm shoulder peak and the predominant 675 nm peak in Ce_2@C_{72} become nearly imperceptible in the UCCe@C_{72} spectrum. These results reveal the substantial impact of U on the electronic structures of endohedral fullerenes.

https://doi.org/10.1021/jacs.3c10042
J. Am. Chem. Soc. 2023, 145, 25440−25449

To further corroborate the oxidation state assignments of the encapsulated metal elements for a full representation of the electronic structure and chemical bonding inside the fullerene cages, the Ce-2$p_{3/2}$ and U-2$p_{3/2}$ X-ray absorption spectra of UCCe@C_{78} and several reference compounds were recorded in Figure 2E,F. A dominant shift to higher edge energies occurs from ligation by soft organic π-systems to oxo and chloro anions with more polar bonds. The π-pair donation significantly reduces the effective positive charge on the metal cations. Within each group of ligand environments, the edge energy increases by ~1 eV per formal oxidation number, as indicated by the black arrows. Hence, the observed spectra suggest a formal charge assignment of U^{6+} and Ce^{4+} for UCCe@C_{78}, which is in line with the common electronegativities of the elements (U/Ce ≈ 1.2)[50] as well as with the calculated effective averaged atomic charge distribution of UCCe@C_{2n} (Table S5).

Computational Studies of Molecular Structure and Bonding in UCCe@C_{2n}. To elucidate the chemical bonding and electronic structure of UCCe@C_{2n} and to explore the role of the fullerene cages for EMF formation, quantum-chemical studies were conducted for UCCe@C_{2n} and for model complexes LUCCeL (L = C_7H_7 or H_3). Theoretical calculations using density functional theory (DFT) were used to derive the canonical molecular orbitals (MOs), electron density distributions, effective charges, interaction energies, localized bonding, and bond multiplicities.

Insight into the bonding of endohedral bimetallic carbide UCCe clusters is provided by natural localized molecular orbitals (NLMOs). The four electron pairs on the carbon of the UCCe unit form four optimally localized MOs, two σ_z-pairs, and two π_x and π_y pairs (with UCCe along the z-axis). The atomic orbital (AO) contributions of the NLMOs for UCCe@C_{2n} ($2n$ = 72 and 78) are displayed in Figure 3. For

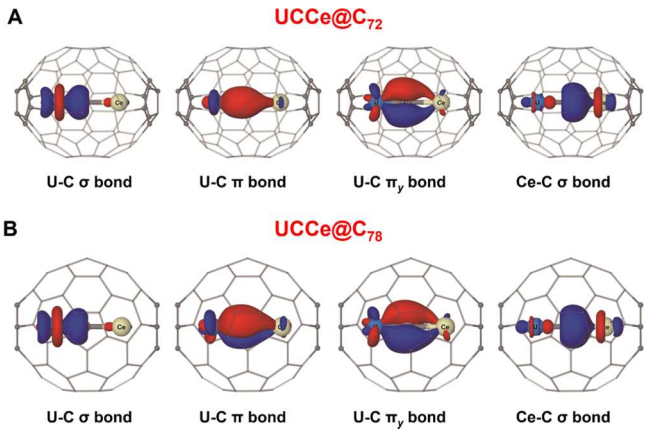

Figure 3. Four natural localized molecular orbitals (NLMOs) on the endohedral UCCe unit for (A) UCCe@C_{72} and (B) UCCe@C_{78}. The value of isosurfaces is ±0.05 a.u. at the B3LYP level.

UCCe@C_{72} (Figure 3A), one σ pair forms a two-center U−C covalent bond, with U(5f6d) and C(2sp) hybrids in almost equal proportions. The two U−C $\pi_{x,y}$ pairs with 53% C-2p AOs mixed with 38% U AOs extend a bit into Ce (8%), showing a slight three-center character. The other localized σ pair also displays a three-center character with a dominant density (66%) on the central C atom and smaller contributions on Ce (23%) and U (9%). The summed-up bond order indices indicate a triple U≡C bond (one σ and two π) and a single bond for the comparatively short C−Ce distance due to the slight three-center character.[51]

UCCe@C_{78} shows a similar bonding pattern for U≡C−Ce as in UCCe@C_{72} (Figure 3B), which is further supported by both the principal interacting orbital (PIO) analysis (Figure S6) and adaptive natural density portioning (AdNDP) analysis (Figure S7). PIO analysis using U and C−Ce as fragments reveals that there is a U≡C triple bond consisting of one σ and two π bonds, with each accounting for ~30%. The U−C π bond is slightly more polar than the U−C σ bond. Furthermore, AdNDP analysis also exhibits a similar two-center U−C σ bond and two 3-center U−C(→Ce) π_x and π_y bonds. The calculated bond indices (Table S6) suggest a bond order of nearly three for U≡C and slightly more than one for C−Ce, consistent with the experimental distances.

Based on DFT calculations, the MO energy-level schemes for UCCe@C_{2n} are shown in Figure 4. Briefly, the central C

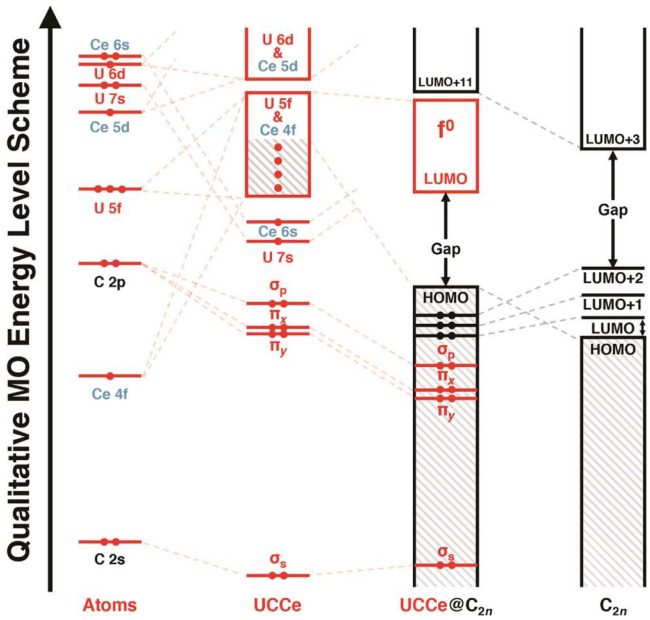

Figure 4. Molecular orbital energy-level scheme for UCCe@C_{2n}. *Left*: (endohedral) atomic valence orbital energy levels C-2s/2p, Ce-4f/5d/6s, and U-5f/6d/7s. *Middle-Left*: ⋮U≡C−Ce⋮ unit. *Right*: C_{2n} fullerenes (D_2(10611)-C_{72} or D_{3h}(5)-C_{78}). *Middle-Right*: compound UCCe@C_{2n} molecules. Occupied orbital energy ranges are hatched. Orbital levels dominated by the endohedral U/C/Ce atoms are shown in red, dominated by the fullerene C atoms in black.

atom in the endohedral cluster can form four electron-pair bonds to its two adjacent metal atoms, U and Ce, leaving six electrons with U/Ce (left panel of Figure 4). Upon encapsulating UCCe into C_{72} or C_{78} cages, the corresponding three lowest unoccupied MOs of the C_{2n} cage accept six electrons from U/Ce (Figures S8−9), yielding formal $[UCCe]^{6+}$ inside $[C_{2n}]^{6-}$ and oxidation numbers, as shown in $[U^{VI}{\equiv}C{-}Ce^{IV}]^{6+}@C_{2n}{}^{6-}$. In addition, the EMF MOs have significant metal contributions (Figure S10), suggesting orbital interactions between U/Ce and C_{2n}, which is also confirmed by PIO analysis (Figure S11) and the contour line diagrams of NLMOs (Figure S12).

Our theoretical analyses indicate that the hexavalent C_{2n} fullerene cages help to stabilize [U≡C−Ce] species with U(VI) and Ce(IV) inside the cages based on four factors: the effective coordinative interactions, charge transfer, appropriate

https://doi.org/10.1021/jacs.3c10042
J. Am. Chem. Soc. 2023, 145, 25440−25449

fullerene size, and the matrix-like cage environment that protect the U≡C−Ce species against redox lability. The unique fullerene cages serve as a protective ligand to stabilize elusive actinide multiple bonding.

CONCLUSIONS

In summary, we present the synthesis, isolation, and characterization of two systems possessing uranium−carbon triple bonds found in the cerium-capped clusters of the EMFs of UCCe@C_{2n} ($2n$ = 72 and 78). Solid-state molecular characterization by X-ray crystallographic analysis reveals the shortest uranium−carbon bonds reported to date in an isolable molecular complex. Indeed, the U≡C bonds (1.921(6) and 1.930(6) Å) are significantly shorter than those reported for the carbeno methanide complex ($[O{=}U{=}CR_2]Cl_2$) (2.184(3) Å) and shorter than the U=C bonds (2.028(5) and 2.033(5) Å) in $U_2C@C_{80}$. The computational model agrees well with the empirical data, further confirming the uranium−carbon triple bonds. The joint experimental and theoretical investigation shows that the endohedral [U≡C−Ce] unit and [C_{2n}] fullerene cages synergistically combine to fit each other geometrically without appreciable strain. The stabilities of the triatomic U≡C−Ce unit are enhanced by charge transfer and coordinative donation of fullerene π-pairs to the metal atoms, leading to formal charge C_{2n}^{6-} and corresponding U^{6+} and Ce^{4+} oxidation states. Our success of the synthesis of UCCe@C_{2n} ($2n$ = 72 and 78) further establishes the feasibility of using fullerene cages for trapping and accessing molecular complexes featuring elusive and reactive actinide−ligand multiple bonds. This method opens up opportunities to create model compounds for further studies in this field that may provide critical insights into the synthetic design and electronic properties of nonfullerene compounds with similar bonding motifs. Enhancing our fundamental understanding of the chemical properties of the actinide elements is crucial for improving the nuclear fuel cycle, necessary for advancing carbon-free energy technologies, and also for developing improved methods for the environmental remediation of these elements.

EXPERIMENTAL SECTION

Synthesis and Isolation. UCCe@C_{2n} ($2n$ = 72 and 78) was synthesized by a modified Krätschmer−Huffman direct-current arc-discharge method. Briefly, a drilled graphite rod, fully packed with a mixture containing graphite powder, U_3O_8, and CeO_2 (molar ratio of C:U:Ce = 24:1:1), was installed in a VDK250 arcing reactor (Beijing Technol Science Co., Ltd., China) as the anode under a 200 Torr atmosphere and then arced with a graphite cathode under a 100 A direct current, yielding the products of carbon soot. The targeted U-based metallofullerenes were extracted from the carbon soot by CS_2 for 24 h and then isolated using an LC-9204 recycling preparative HPLC system (Japan Analytical Industry Co., Ltd., Japan). Five types of Cosmosil columns (Nacalai Tesque Inc., Japan), including a preparative Buckyprep-M (20 × 250 mm), a semipreparative Buckyprep-M (10 × 250 mm), a semipreparative Buckprep (10 × 250 mm), a semipreparative 5PYE (10 × 250 mm), and a semipreparative 5PBB (10 × 250 mm), were utilized in the HPLC procedures.

Spectroscopic Studies. Mass spectra of UCCe@C_{2n} were recorded on a Microflex LRF matrix-assisted laser desorption/ionization time-of-flight (MALDI-TOF, Bruker Daltonics Inc., U.S.) spectrometer using the positive-ion mode. The vis−NIR absorption spectra of the purified UCCe@C_{2n} molecules dissolved in toluene were recorded on a Cary5000 spectrometer (Agilent Technologies Co., Ltd., U.S.) in the range 400−1600 nm. The FTIR spectra of the purified UCCe@C_{2n} solids were recorded on a Vertex 70 spectrometer (Bruker Daltonics Inc., U.S.) at room temperature with a resolution of 2 cm^{-1}. The XANES spectra of purified UCCe@C_{78} and other reference compounds were performed at the BL14W1 XAS beamline of the Shanghai Synchrotron Radiation Facility (SSRF). The samples were prepared into a hole of a perforated polytetrafluoroethylene (PTFE) film (film thickness: ca. 0.3 mm, hole diameter: ca. 1 mm).

Single-Crystal X-ray Diffraction. Black block crystals of UCCe@C_{2n} were obtained by a slow diffusion cocrystallization method. The CS_2 solution of the samples was slowly diffused into a benzene solution of Ni^{II}(OEP)[52] (OEP = 2, 3, 7, 8, 12, 13, 17, 18-octaethylporphyrin dianion), yielding black block cocrystals suitable for SC-XRD studies after ca. 3 weeks. The crystallographic data were recorded on a Bruker D8 Venture single-crystal X-ray diffractometer (Bruker Daltonics Inc., U.S.) equipped with Mo Kα radiation (0.71073 Å) at 100 K. The refinement of the crystallographic structures was performed in the Olex2 software[53] packed with SHELXL-2018[54] by the full-matrix least-squares method. The supplementary crystallographic data for this paper can be obtained free of charge from the Cambridge Crystallographic Data Centre with CCDC numbers 2239921 and 2239922 via www.ccdc.cam.ac.uk/data_request/cif.

Quantum Computational Methods. The geometries and vibrational frequencies (starting with the XRD geometric structures) were calculated for different spin states of the UCCe@C_{2n} molecules (Tables S7−8). The generalized gradient approximation (GGA), meta-GGA, and hybrid-GGA Kohn−Sham density functional (DF) approximations were applied, using the PBE[55,56] with or without the dispersion correction of the Becke−Johnson damping scheme (D3BJ),[57,58] the MN15L[59] and B3LYP,[60] and the PBE0[61] functionals. The ADF-2019[62,63] and the Gaussian-16[64] program packages were applied.

With ADF-2019, the scalar relativistic effects were simulated with the zero-order regular approximation (ZORA).[65−67] Slater-type orbital (STO) basis sets of triple-ζ plus two polarization functions' (TZ2P) quality[68] were employed for the endohedral atoms. Double zeta-polarized (DZP) basis sets were used for the caged carbon atoms. With Gaussian-16, the Stuttgart−Dresden−Cologne quasi-relativistic effective core potentials, including ECP60MWB[69] for U and ECP28MWB[70] for Ce, with the adapted basis sets, were used. The double-ζ 6−31G* basis set for all C atoms[71,72] was applied. The vibrational frequencies in terms of IR wavenumbers were computed in the harmonic approximation, with the MN15L functional, and then scaled by a factor of 0.96, which was reproduced from the experimental frequency of the free C≡O molecule (2143 cm^{-1}). For the FTIR absorption curves, the Lorentzian line shape function with 4 cm^{-1} full width at half-maximum was applied to all lines.

With ADF-2019, bond order analyses, including the Mayer bond order,[73] the Gopinathan−Jug bond order,[74] and the Nalewajski−Mrozek bond order No. 3,[75] and an effective charge analysis were obtained. Natural localized molecular orbitals (NLMO) and the Wiberg bond index (WBI)[76] were obtained from the NBO-6.0 program.[77] Adaptive natural density portioning (AdNDP),[78] Pipek's delocalized index (DI), and 'quantum theory of atoms in molecules' (QATAM)[79] analyses were obtained from the Multiwfn program,[80] using the results from the B3LYP density functional throughout.

ASSOCIATED CONTENT

Supporting Information

The Supporting Information is available free of charge at https://pubs.acs.org/doi/10.1021/jacs.3c10042.

Mass spectra, HPLC isolation procedures, crystallographic information, and additional calculation analysis of UCCe@C_{2n} ($2n$ = 72 and 78) (PDF).

Accession Codes

CCDC 2239921−2239922 contain the supplementary crystallographic data for this paper. These data can be obtained

https://doi.org/10.1021/jacs.3c10042
J. Am. Chem. Soc. 2023, 145, 25440−25449

free of charge via www.ccdc.cam.ac.uk/data_request/cif, or by emailing data_request@ccdc.cam.ac.uk, or by contacting The Cambridge Crystallographic Data Centre, 12 Union Road, Cambridge CB2 1EZ, UK; fax: +44 1223 336033.

AUTHOR INFORMATION

Corresponding Authors

Jun Li − *Department of Chemistry and Engineering Research Center of Advanced Rare-Earth Materials of the Ministry of Education, Tsinghua University, Beijing 100084, China; Department of Chemistry and Guangdong Provincial Key Laboratory of Catalytic Chemistry, Southern University of Science and Technology, Shenzhen 518055, China;* orcid.org/0000-0002-8456-3980; Email: junli@tsinghua.edu.cn

Ning Chen − *College of Chemistry, Chemical Engineering and Materials Science & State Key Laboratory of Radiation Medicine and Protection, Soochow University, Suzhou 215123, China;* orcid.org/0000-0002-9405-6229; Email: chenning@suda.edu.cn

Authors

Yang-Rong Yao − *College of Chemistry, Chemical Engineering and Materials Science & State Key Laboratory of Radiation Medicine and Protection, Soochow University, Suzhou 215123, China;* orcid.org/0000-0003-3495-1691

Jing Zhao − *Department of Chemistry and Engineering Research Center of Advanced Rare-Earth Materials of the Ministry of Education, Tsinghua University, Beijing 100084, China*

Qingyu Meng − *College of Chemistry, Chemical Engineering and Materials Science & State Key Laboratory of Radiation Medicine and Protection, Soochow University, Suzhou 215123, China*

Han-Shi Hu − *Department of Chemistry and Engineering Research Center of Advanced Rare-Earth Materials of the Ministry of Education, Tsinghua University, Beijing 100084, China;* orcid.org/0000-0001-9508-1920

Min Guo − *College of Chemistry, Chemical Engineering and Materials Science & State Key Laboratory of Radiation Medicine and Protection, Soochow University, Suzhou 215123, China*

Yingjing Yan − *College of Chemistry, Chemical Engineering and Materials Science & State Key Laboratory of Radiation Medicine and Protection, Soochow University, Suzhou 215123, China*

Jiaxin Zhuang − *College of Chemistry, Chemical Engineering and Materials Science & State Key Laboratory of Radiation Medicine and Protection, Soochow University, Suzhou 215123, China*

Shangfeng Yang − *Department of Materials Science and Engineering, CAS Key Laboratory of Materials for Energy Conversion, Anhui Laboratory of Advanced Photon Science and Technology, University of Science and Technology of China, Hefei 230026, China;* orcid.org/0000-0002-6931-9613

Skye Fortier − *Department of Chemistry and Biochemistry, University of Texas at El Paso, El Paso, Texas 79968, United States;* orcid.org/0000-0002-0502-5229

Luis Echegoyen − *Institut Catalá d'Investigació Química, 43007 Tarragona, Spain; Department of Chemistry and Biochemistry, University of Texas at El Paso, El Paso, Texas 79968, United States;* orcid.org/0000-0003-1107-9423

W. H. Eugen Schwarz − *Department of Chemistry and Engineering Research Center of Advanced Rare-Earth Materials of the Ministry of Education, Tsinghua University, Beijing 100084, China; Physikalische und Theoretische Chemie, Universität Siegen, Siegen 57068, Germany*

Complete contact information is available at: https://pubs.acs.org/10.1021/jacs.3c10042

Author Contributions

○Y.-R.Y., J.Z., and Q.M. contributed equally to this work.

Author Contributions

The manuscript was written through contributions of all authors. All authors have given approval to the final version of the manuscript.

Notes

The authors declare no competing financial interest.

ACKNOWLEDGMENTS

This work was supported by the National Natural Science Foundation of China (NSFC Nos. 9196110, 52172051, 22033005, 22222605, 22301288, and 51925206), Natural Science Foundation of Jiangsu Province (BK20200041), Priority Academic Program Development of Jiangsu Higher Education Institutions (PAPD), Guangdong Provincial Key Laboratory of Catalysis (2020B121201002), Anhui Provincial Natural Science Foundation (2308085MB31), Fundamental Research Funds for the Central Universities (WK2060000051), the U.S. National Science Foundation (CHE-1801317), and the Robert A. Welch Foundation (grant AH-0033 and AH-1922-20230405). We also thank the Shanghai Synchrotron Radiation Facility (SSRF) for the kind technique support of the XAS test.

REFERENCES

(1) Liddle, S. T. The Renaissance of Non-Aqueous Uranium Chemistry. *Angew. Chem., Int. Ed.* **2015**, *54* (30), 8604−8641.

(2) Nugent, W. A.; Mayer, J. M., *Metal-ligand multiple bonds: the chemistry of transition metal complexes containing oxo, nitrido, imido, alkylidene, or alkylidyne ligands*; Wiley: New York: New York, **1988**.

(3) Vitova, T.; Pidchenko, I.; Fellhauer, D.; Bagus, P. S.; Joly, Y.; Pruessmann, T.; Bahl, S.; Gonzalez-Robles, E.; Rothe, J.; Altmaier, M.; Denecke, M. A.; Geckeis, H. The role of the 5f valence orbitals of early actinides in chemical bonding. *Nat. Commun.* **2017**, *8* (1), 16053.

(4) Motta, L. C.; Autschbach, J. Actinide inverse trans influence versus cooperative pushing from below and multi-center bonding. *Nat. Commun.* **2023**, *14* (1), 4307.

(5) Denning, R. G. Electronic Structure and Bonding in Actinyl Ions and their Analogs. *J. Phys. Chem. A* **2007**, *111* (20), 4125−4143.

(6) Hayton, T. W. Metal-ligand multiple bonding in uranium: structure and reactivity. *Dalton Trans.* **2010**, *39* (5), 1145−1158.

(7) Hayton, T. W. Recent developments in actinide-ligand multiple bonding. *Chem. Commun.* **2013**, *49* (29), 2956−73.

(8) Schädle, D.; Anwander, R. Rare-earth metal and actinide organoimide chemistry. *Chem. Soc. Rev.* **2019**, *48* (24), 5752−5805.

(9) Jones, M. B.; Gaunt, A. J. Recent Developments in Synthesis and Structural Chemistry of Nonaqueous Actinide Complexes. *Chem. Rev.* **2013**, *113* (2), 1137−1198.

(10) Fortier, S.; Walensky, J. R.; Wu, G.; Hayton, T. W. Synthesis of a Phosphorano-Stabilized U(IV)-Carbene via One-Electron Oxidation of a U(III)-Ylide Adduct. *J. Am. Chem. Soc.* **2011**, *133* (18), 6894−6897.

(11) Mills, D. P.; Cooper, O. J.; Tuna, F.; McInnes, E. J. L.; Davies, E. S.; McMaster, J.; Moro, F.; Lewis, W.; Blake, A. J.; Liddle, S. T. Synthesis of a Uranium(VI)-Carbene: Reductive Formation of

Uranyl(V)-Methanides, Oxidative Preparation of a $[R_2C=U=O]^{2+}$ Analogue of the $[O=U=O]^{2+}$ Uranyl Ion (R = $Ph_2PNSiMe_3$), and Comparison of the Nature of U^{IV}=C, U^{V}=C, and U^{VI}=C Double Bonds. *J. Am. Chem. Soc.* **2012**, *134* (24), 10047−10054.
(12) Cantat, T.; Arliguie, T.; Noël, A.; Thuéry, P.; Ephritikhine, M.; Floch, P. L.; Mézailles, N. The U=C Double Bond: Synthesis and Study of Uranium Nucleophilic Carbene Complexes. *J. Am. Chem. Soc.* **2009**, *131* (3), 963−972.
(13) Gregson, M.; Lu, E.; Mills, D. P.; Tuna, F.; McInnes, E. J. L.; Hennig, C.; Scheinost, A. C.; McMaster, J.; Lewis, W.; Blake, A. J.; Kerridge, A.; Liddle, S. T. The inverse-trans-influence in tetravalent lanthanide and actinide bis(carbene) complexes. *Nat. Commun.* **2017**, *8* (1), 14137.
(14) Anderson, N. H.; Odoh, S. O.; Yao, Y.; Williams, U. J.; Schaefer, B. A.; Kiernicki, J. J.; Lewis, A. J.; Goshert, M. D.; Fanwick, P. E.; Schelter, E. J.; Walensky, J. R.; Gagliardi, L.; Bart, S. C. Harnessing redox activity for the formation of uranium tris(imido) compounds. *Nat. Chem.* **2014**, *6* (10), 919−926.
(15) Anderson, N. H.; Xie, J.; Ray, D.; Zeller, M.; Gagliardi, L.; Bart, S. C. Elucidating bonding preferences in tetrakis(imido)uranate(VI) dianions. *Nat. Chem.* **2017**, *9* (9), 850−855.
(16) Hayton, T. W.; Boncella, J. M.; Scott, B. L.; Palmer, P. D.; Batista, E. R.; Hay, P. J. Synthesis of Imido Analogs of the Uranyl Ion. *Science* **2005**, *310* (5756), 1941−1943.
(17) Evans, W. J.; Kozimor, S. A.; Ziller, J. W. Molecular Octa-Uranium Rings with Alternating Nitride and Azide Bridges. *Science* **2005**, *309* (5742), 1835−1838.
(18) King, D. M.; Tuna, F.; McInnes, E. J. L.; McMaster, J.; Lewis, W.; Blake, A. J.; Liddle, S. T. Isolation and characterization of a uranium(VI)−nitride triple bond. *Nat. Chem.* **2013**, *5* (6), 482−488.
(19) King, D. M.; Tuna, F.; McInnes, E. J. L.; McMaster, J.; Lewis, W.; Blake, A. J.; Liddle, S. T. Synthesis and Structure of a Terminal Uranium Nitride Complex. *Science* **2012**, *337* (6095), 717−720.
(20) Patel, D.; Tuna, F.; McInnes, E. J. L.; Lewis, W.; Blake, A. J.; Liddle, S. T. An Actinide Zintl Cluster: A Tris(triamidouranium)μ^3-η^2:η^2:η^2-Heptaphosphanortricyclane and Its Diverse Synthetic Utility. *Angew. Chem., Int. Ed.* **2013**, *52* (50), 13334−13337.
(21) Gardner, B. M.; Balázs, G.; Scheer, M.; Tuna, F.; McInnes, E. J. L.; McMaster, J.; Lewis, W.; Blake, A. J.; Liddle, S. T. Triamidoamine−Uranium(IV)-Stabilized Terminal Parent Phosphide and Phosphinidene Complexes. *Angew. Chem., Int. Ed.* **2014**, *53* (17), 4484−4488.
(22) Gardner, B. M.; Balázs, G.; Scheer, M.; Tuna, F.; McInnes, E. J. L.; McMaster, J.; Lewis, W.; Blake, A. J.; Liddle, S. T. Triamidoamine uranium(IV)−arsenic complexes containing one-, two- and threefold U−As bonding interactions. *Nat. Chem.* **2015**, *7* (7), 582−590.
(23) Dutkiewicz, M. S.; Goodwin, C. A. P.; Perfetti, M.; Gaunt, A. J.; Griveau, J.-C.; Colineau, E.; Kovács, A.; Wooles, A. J.; Caciuffo, R.; Walter, O.; Liddle, S. T. A terminal neptunium(V)−mono(oxo) complex. *Nat. Chem.* **2022**, *14* (3), 342−349.
(24) King, D. M.; Tuna, F.; McMaster, J.; Lewis, W.; Blake, A. J.; McInnes, E. J. L.; Liddle, S. T. Single-Molecule Magnetism in a Single-Ion Triamidoamine Uranium(V) Terminal Mono-Oxo Complex. *Angew. Chem., Int. Ed.* **2013**, *52* (18), 4921−4924.
(25) Fortier, S.; Kaltsoyannis, N.; Wu, G.; Hayton, T. W. Probing the Reactivity and Electronic Structure of a Uranium(V) Terminal Oxo Complex. *J. Am. Chem. Soc.* **2011**, *133* (36), 14224−14227.
(26) Fortier, S.; Hayton, T. W. Oxo ligand functionalization in the uranyl ion (UO_2^{2+}). *Coord. Chem. Rev.* **2010**, *254* (3), 197−214.
(27) Smiles, D. E.; Wu, G.; Hrobárik, P.; Hayton, T. W. Use of ^{77}Se and ^{125}Te NMR Spectroscopy to Probe Covalency of the Actinide-Chalcogen Bonding in $[Th(E_n)\{N(SiMe_3)_2\}_3]^-$ (E = Se, Te; *n* = 1, 2) and Their Oxo-Uranium(VI) Congeners. *J. Am. Chem. Soc.* **2016**, *138* (3), 814−825.
(28) Brown, J. L.; Fortier, S.; Lewis, R. A.; Wu, G.; Hayton, T. W. A Complete Family of Terminal Uranium Chalcogenides, $[U(E)(N\{SiMe_3\}_2)_3]^-$ (E = O, S, Se, Te). *J. Am. Chem. Soc.* **2012**, *134* (37), 15468−15475.
(29) Brown, J. L.; Fortier, S.; Wu, G.; Kaltsoyannis, N.; Hayton, T. W. Synthesis and Spectroscopic and Computational Characterization of the Chalcogenido-Substituted Analogues of the Uranyl Ion, $[OUE]^{2+}$ (E = S, Se). *J. Am. Chem. Soc.* **2013**, *135* (14), 5352−5355.
(30) Gregson, M.; Wooles, A. J.; Cooper, O. J.; Liddle, S. T. Covalent Uranium Carbene Chemistry. *Comments Inorg. Chem.* **2015**, *35* (5), 262−294.
(31) Lyon, J. T.; Hu, H.-S.; Andrews, L.; Li, J. Formation of unprecedented actinide≡carbon triple bonds in uranium methylidyne molecules. *Proc. Natl. Acad. Sci. U. S. A.* **2007**, *104* (48), 18919−24.
(32) Wang, X.; Andrews, L.; Malmqvist, P.-Å.; Roos, B. O.; Gonçalves, A. P.; Pereira, C. C. L.; Marçalo, J.; Godart, C. Infrared Spectra and Quantum Chemical Calculations of the Uranium Carbide Molecules UC and CUC with Triple Bonds. *J. Am. Chem. Soc.* **2010**, *132* (24), 8484−8488.
(33) Kent, G. T.; Yu, X.; Wu, G.; Autschbach, J.; Hayton, T. W. Synthesis and electronic structure analysis of the actinide allenylidenes, $[\{(NR_2)_3\}An(CCCPh_2)]^-$ (An = U, Th; R = $SiMe_3$). *Chem. Sci.* **2021**, *12* (43), 14383−14388.
(34) Seed, J. A.; Sharpe, H. R.; Futcher, H. J.; Wooles, A. J.; Liddle, S. T. Nature of the Arsonium-Ylide $Ph_3As=CH_2$ and a Uranium(IV) Arsonium-Carbene Complex. *Angew. Chem., Int. Ed.* **2020**, *59* (37), 15870−15874.
(35) Zhang, X.; Li, W.; Feng, L.; Chen, X.; Hansen, A.; Grimme, S.; Fortier, S.; Sergentu, D.-C.; Duignan, T. J.; Autschbach, J.; Wang, S.; Wang, Y.; Velkos, G.; Popov, A. A.; Aghdassi, N.; Duhm, S.; Li, X.; Li, J.; Echegoyen, L.; Schwarz, W. H. E.; Chen, N. A diuranium carbide cluster stabilized inside a C_{80} fullerene cage. *Nat. Commun.* **2018**, *9* (1), 2753.
(36) Zhuang, J.; Abella, L.; Sergentu, D.-C.; Yao, Y.-R.; Jin, M.; Yang, W.; Zhang, X.; Li, X.; Zhang, D.; Zhao, Y.; Li, X.; Wang, S.; Echegoyen, L.; Autschbach, J.; Chen, N. Diuranium(IV) Carbide Cluster U_2C_2 Stabilized Inside Fullerene Cages. *J. Am. Chem. Soc.* **2019**, *141* (51), 20249−20260.
(37) Li, X.; Roselló, Y.; Yao, Y.-R.; Zhuang, J.; Zhang, X.; Rodríguez-Fortea, A.; de Graaf, C.; Echegoyen, L.; Poblet, J. M.; Chen, N. U_2N@I_h(7)-C_{80}: fullerene cage encapsulating an unsymmetrical U(IV)=N=U(V) cluster. *Chem. Sci.* **2021**, *12* (1), 282−292.
(38) Meng, Q.; Abella, L.; Yang, W.; Yao, Y.-R.; Liu, X.; Zhuang, J.; Li, X.; Echegoyen, L.; Autschbach, J.; Chen, N. UCN@C_s(6)-C_{82}: An Encapsulated Triangular UCN Cluster with Ambiguous U Oxidation State [U(III) versus U(I)]. *J. Am. Chem. Soc.* **2021**, *143* (39), 16226−16234.
(39) Yao, Y.-R.; Roselló, Y.; Ma, L.; Puente Santiago, A. R.; Metta-Magaña, A.; Chen, N.; Rodríguez-Fortea, A.; Poblet, J. M.; Echegoyen, L. Crystallographic Characterization of U@C_{2n} (2*n* = 82−86): Insights about Metal-Cage Interactions for Mono-metallofullerenes. *J. Am. Chem. Soc.* **2021**, *143* (37), 15309−15318.
(40) Zhuang, J.; Morales-Martínez, R.; Zhang, J.; Wang, Y.; Yao, Y.-R.; Pei, C.; Rodríguez-Fortea, A.; Wang, S.; Echegoyen, L.; de Graaf, C.; Poblet, J. M.; Chen, N. Characterization of a strong covalent Th^{3+}-Th^{3+} bond inside an I_h(7)-C_{80} fullerene cage. *Nat. Commun.* **2021**, *12* (1), 2372.
(41) Jiang, H.; Yu, X.; Guo, M.; Yao, Y.-R.; Meng, Q.; Echegoyen, L.; Autschbach, J.; Chen, N. USc_2C_2 and USc_2NC Clusters with U-C Triple Bond Character Stabilized Inside Fullerene Cages. *J. Am. Chem. Soc.* **2023**, *145* (10), 5645−5654.
(42) Meng, Q.; Abella, L.; Yao, Y.-R.; Sergentu, D.-C.; Yang, W.; Liu, X.; Zhuang, J.; Echegoyen, L.; Autschbach, J.; Chen, N. A charged diatomic triple-bonded U≡N species trapped in C_{82} fullerene cages. *Nat. Commun.* **2022**, *13* (1), 7192.
(43) Krätschmer, W.; Lamb, L. D.; Fostiropoulos, K.; Huffman, D. R. Solid C_{60}: a new form of carbon. *Nature* **1990**, *347* (6291), 354−358.
(44) Kroto, H. W. The stability of the fullerenes C_n, with *n* = 24, 28, 32, 36, 50, 60 and 70. *Nature* **1987**, *329* (6139), 529−531.
(45) Fowler, P. W.; Manolopoulos, D. E., *An atlas of fullerenes*; Clarendon Press; Oxford University Press: Oxford; New York, 1995.

https://doi.org/10.1021/jacs.3c10042
J. Am. Chem. Soc. 2023, 145, 25440−25449

(46) Pyykkö, P. Additive Covalent Radii for Single-, Double-, and Triple-Bonded Molecules and Tetrahedrally Bonded Crystals: A Summary. *J. Phys. Chem. A* **2015**, *119* (11), 2326−2337.
(47) Popov, A. A.; Kästner, C.; Krause, M.; Dunsch, L. Carbon Cage Vibrations of M@C_{82} and M_2@C_{2n} (M = La, Ce; 2*n* = 72, 78, 80): The Role of the Metal Atoms. *Fuller. Nanotub. Carbon Nanostruct.* **2014**, *22* (1−3), 202−214.
(48) Popov, A. A.; Yang, S.; Dunsch, L. Endohedral Fullerenes. *Chem. Rev.* **2013**, *113* (8), 5989−6113.
(49) Yamada, M.; Wakahara, T.; Tsuchiya, T.; Maeda, Y.; Akasaka, T.; Mizorogi, N.; Nagase, S. Spectroscopic and Theoretical Study of Endohedral Dimetallofullerene Having a Non-IPR Fullerene Cage: Ce_2@C_{72}. *J. Phys. Chem. A* **2008**, *112* (33), 7627−7631.
(50) Allred, A. L. Electronegativity values from thermochemical data. *J. Inorg. Nucl. Chem.* **1961**, *17* (3), 215−221.
(51) Here, we stress the conceptual difference between multiple bond order and multiple bond character. The ″U−C triple bond character″ mentioned in Ref. (41) means that three (more or less) polycentric LMOs (localized molecular orbitals) each contribute significantly to the U-C interaction, summing up to a bond strength of double order in chemical terms. In contrast, the present ″U−C triple bond order″ indicates a respectively shorter bond length, larger bond-energy increment and larger local force constant, caused by four LMOs.
(52) Olmstead, M. M.; Costa, D. A.; Maitra, K.; Noll, B. C.; Phillips, S. L.; Van Calcar, P. M.; Balch, A. L. Interaction of Curved and Flat Molecular Surfaces. The Structures of Crystalline Compounds Composed of Fullerene (C_{60}, C_{60}O, C_{70}, and C_{120}O) and Metal Octaethylporphyrin Units. *J. Am. Chem. Soc.* **1999**, *121* (30), 7090−7097.
(53) Paquette, L. A. Dodecahedrane—The chemical transliteration of Plato's universe (A Review). *Proc. Natl. Acad. Sci. U. S. A.* **1982**, *79* (14), 4495.
(54) Sheldrick, G. Crystal structure refinement with SHELXL. *Acta Crystallogr. Sect. C Struct. Chem.* **2015**, *71* (1), 3−8.
(55) Ernzerhof, M.; Scuseria, G. E. Assessment of the Perdew−Burke−Ernzerhof exchange-correlation functional. *J. Chem. Phys.* **1999**, *110* (11), 5029−5036.
(56) Hammer, B.; Hansen, L. B.; Nørskov, J. K. Improved adsorption energetics within density-functional theory using revised Perdew-Burke-Ernzerhof functionals. *Phys. Rev. B* **1999**, *59* (11), 7413−7421.
(57) Grimme, S.; Ehrlich, S.; Goerigk, L. Effect of the damping function in dispersion corrected density functional theory. *J. Comput. Chem.* **2011**, *32* (7), 1456−1465.
(58) Becke, A. D.; Johnson, E. R. A density-functional model of the dispersion interaction. *J. Chem. Phys.* **2005**, *123* (15), 154101.
(59) Yu, H. S.; He, X.; Truhlar, D. G. MN15-L: A New Local Exchange-Correlation Functional for Kohn−Sham Density Functional Theory with Broad Accuracy for Atoms, Molecules, and Solids. *J. Chem. Theory Comput.* **2016**, *12* (3), 1280−1293.
(60) Stephens, P. J.; Devlin, F. J.; Chabalowski, C. F.; Frisch, M. J. Ab Initio Calculation of Vibrational Absorption and Circular Dichroism Spectra Using Density Functional Force Fields. *J. Phys. Chem.* **1994**, *98* (45), 11623−11627.
(61) Adamo, C.; Barone, V. Toward reliable density functional methods without adjustable parameters: The PBE0 model. *J. Chem. Phys.* **1999**, *110* (13), 6158−6170.
(62) te Velde, G.; Bickelhaupt, F. M.; Baerends, E. J.; Fonseca Guerra, C.; van Gisbergen, S. J. A.; Snijders, J. G.; Ziegler, T. Chemistry with ADF. *J. Comput. Chem.* **2001**, *22* (9), 931−967.
(63) Baerends, E. J.; Ziegler, T.; Atkins, A. J.; Autschbach, J.; Bashford, D.; Baseggio, O.; Brces, A.; Bickelhaupt, F. M.; Bo, C.; Boerritger, P. M.; Cavallo, L.; Daul, C.; Chong, D. P.; Chulhai, D. V.; Deng, L.; Dickson, R. M.; Dieterich, J. M.; Ellis, D. E.; van Faassen, M.; Ghysels, A.; Giammona, A.; van Gisbergen, S. J. A.; Goez, A.; Gtz, A. W.; Gusarov, S.; Harris, F. E.; van den Hoek, P.; Hu, Z.; Jacob, C. R.; Jacobsen, H.; Jensen, L.; Joubert, L.; Kaminski, J. W.; van Kessel, G.; Knig, C.; Kootstra, F.; Kovalenko, A.; Krykunov, M.; van Lenthe, E.; McCormack, D. A.; Michalak, A.; Mitoraj, M.; Morton, S. M.; Neugebauer, J.; Nicu, V. P.; Noodleman, L.; Osinga, V. P.; Patchkovskii, S.; Pavanello, M.; Peeples, C. A.; Philipsen, P. H. T.; Post, D.; Pye, C. C.; Ramanantoanina, H.; Ramos, P.; Ravenek, W.; Rodrguez, J. I.; Ros, P.; Rger, R.; Schipper, P. R. T.; Schlns, D.; van Schoot, H.; Schreckenbach, G.; Seldenthuis, J. S.; Seth, M.; Snijders, J. G.; *Sol ADF2019, SCM, Theoretical Chemistry*; Vrije Universiteit, The Netherlands: Amsterdam, 2019.
(64) Frisch, M. J.; Trucks, G. W.; Schlegel, H. B.; Scuseria, G. E.; Robb, M. A.; Cheeseman, J. R.; Scalmani, G.; Barone, V.; Petersson, G. A.; Nakatsuji, H.; Li, X.; Caricato, M.; Marenich, A. V.; Bloino, J.; Janesko, B. G.; Gomperts, R.; Mennucci, B.; Hratchian, H. P.; Ortiz, J. V.; Izmaylov, A. F.; Sonnenberg, J. L.; Williams; Ding, F.; Lipparini, F.; Egidi, F.; Goings, J.; Peng, B.; Petrone, A.; Henderson, T.; Ranasinghe, D.; Zakrzewski, V. G.; Gao, J.; Rega, N.; Zheng, G.; Liang, W.; Hada, M.; Ehara, M.; Toyota, K.; Fukuda, R.; Hasegawa, J.; Ishida, M.; Nakajima, T.; Honda, Y.; Kitao, O.; Nakai, H.; Vreven, T.; Throssell, K.; Montgomery, Jr., J. A.; Peralta, J. E.; Ogliaro, F.; Bearpark, M. J.; Heyd, J. J.; Brothers, E. N.; Kudin, K. N.; Staroverov, V. N.; Keith, T. A.; Kobayashi, R.; Normand, J.; Raghavachari, K.; Rendell, A. P.; Burant, J. C.; Iyengar, S. S.; Tomasi, J.; Cossi, M.; Millam, J. M.; Klene, M.; Adamo, C.; Cammi, R.; Ochterski, J. W.; Martin, R. L.; Morokuma, K.; Farkas, O.; Foresman, J. B.; Fox, D. J. *Gaussian 16 Rev. A.03*; Wallingford, CT, 2016.
(65) Lenthe, E. v.; Baerends, E. J.; Snijders, J. G Relativistic regular two-component Hamiltonians. *J. Chem. Phys.* **1993**, *99* (6), 4597−4610.
(66) van Lenthe, E.; Baerends, E. J.; Snijders, J. G. Relativistic total energy using regular approximations. *J. Chem. Phys.* **1994**, *101* (11), 9783−9792.
(67) van Lenthe, E.; Ehlers, A.; Baerends, E.-J. Geometry optimizations in the zero order regular approximation for relativistic effects. *J. Chem. Phys.* **1999**, *110* (18), 8943−8953.
(68) Van Lenthe, E.; Baerends, E. J. Optimized Slater-type basis sets for the elements 1−118. *J. Comput. Chem.* **2003**, *24* (9), 1142−1156.
(69) Dolg, M.; Cao, X. Accurate Relativistic Small-Core Pseudopotentials for Actinides. Energy Adjustment for Uranium and First Applications to Uranium Hydride. *J. Phys. Chem. A* **2009**, *113* (45), 12573−12581.
(70) Dolg, M.; Stoll, H.; Preuss, H. Energy-adjusted ab initio pseudopotentials for the rare earth elements. *J. Chem. Phys.* **1989**, *90* (3), 1730−1734.
(71) Hehre, W. J.; Ditchfield, R.; Pople, J. A. Self—Consistent Molecular Orbital Methods. XII. Further Extensions of Gaussian—Type Basis Sets for Use in Molecular Orbital Studies of Organic Molecules. *J. Chem. Phys.* **1972**, *56* (5), 2257−2261.
(72) Hariharan, P. C.; Pople, J. A. The influence of polarization functions on molecular orbital hydrogenation energies. *Theor. Chim. Acta* **1973**, *28* (3), 213−222.
(73) Mayer, I. Charge, bond order and valence in the AB initio SCF theory. *Chem. Phys. Lett.* **1983**, *97* (3), 270−274.
(74) Gopinathan, M. S.; Jug, K.; Valency, I. A quantum chemical definition and properties. *Theor. Chim. Acta* **1983**, *63* (6), 497−509.
(75) Michalak, A.; DeKock, R. L.; Ziegler, T. Bond Multiplicity in Transition-Metal Complexes: Applications of Two-Electron Valence Indices. *J. Phys. Chem. A* **2008**, *112* (31), 7256−7263.
(76) Wiberg, K. B. Application of the pople-santry-segal CNDO method to the cyclopropylcarbinyl and cyclobutyl cation and to bicyclobutane. *Tetrahedron* **1968**, *24* (3), 1083−1096.
(77) Glendening, E. D.; Landis, C. R.; Weinhold, F. NBO 6.0: Natural bond orbital analysis program. *J. Comput. Chem.* **2013**, *34* (16), 1429−1437.
(78) Zubarev, D. Y.; Boldyrev, A. I. Developing paradigms of chemical bonding: adaptive natural density partitioning. *Phys. Chem. Chem. Phys.* **2008**, *10* (34), 5207−5217.
(79) Firme, C. L.; Antunes, O. A. C.; Esteves, P. M. Relation between bond order and delocalization index of QTAIM. *Chem. Phys. Lett.* **2009**, *468* (4), 129−133.

(80) Lu, T.; Chen, F. Multiwfn: A multifunctional wavefunction analyzer. *J. Comput. Chem.* **2012**, *33* (5), 580−592.

https://doi.org/10.1021/jacs.3c10042
J. Am. Chem. Soc. 2023, 145, 25440−25449